LETTER

Manipulating thermoelectric fields with bilayer schemes beyond Laplacian metamaterials

To cite this article: T. Qu *et al* 2021 *EPL* **135** 54004

View the article online for updates and enhancements.

Manipulating thermoelectric fields with bilayer schemes beyond Laplacian metamaterials

T. Qu[1], J. Wang[1,2(a)] (iD) and J. P. Huang[1(b)] (iD)

[1] *Department of Physics, State Key Laboratory of Surface Physics, and Key Laboratory of Micro and Nano Photonic Structures (MOE), Fudan University - Shanghai 200438, China*
[2] *School of Physics, East China University of Science and Technology - Shanghai 200237, China*

Abstract – Manipulating multiphysical fields with metamaterials has received enormous attention recently because of the high functional integration and extensive practical applicability. However, coupled multi-field systems such as thermoelectric fields, where heat and electric fluxes are coupled via the Seebeck coefficients, still lack efficient control with artificial structures. Here, we theoretically design a category of bilayer thermoelectric metamaterials based on the generalized scattering-cancellation method. By solving the governing equations directly, we formulate the specific parameter requirements for the desired functionalities beyond existing single-field or decoupled multi-field Laplacian metamaterials. Compared with the recently reported transformation optics for thermoelectric flows, bilayer schemes do not require inhomogeneity and anisotropy in constitutive materials. Finite-element simulations confirm the analytical results and show robustness under various exterior conditions. A feasible experimental design with naturally occuring materials is also proposed for further proof-of-principle verification. Our theoretical method and device design may be extended to other coupled multiphysical systems such as thermo-optics, thermomagnetics, optomechanics, etc.

Introduction. – Metamaterials have shown superior control ability beyond naturally occurring materials in both wave [1–9] and diffusion [10–18] systems. The transformation theory [1–4,10,11] and scattering-cancellation method [8,9,12–14], as two common approaches for manipulating physical fields, have achieved great success in artificial structure design. In particular, the latter is based on solving steady-state governing equations directly under given boundary conditions, leading to isotropic and homogeneous design parameters. However, if multiple fields act on an individual system, for example, there exist heat and electric fluxes simultaneously [19–21], the governing equations are hard to handle because of the newly introduced coupling terms induced by thermoelectric (TE) effects. Appropriate theoretical methods need to be developed for designing such multiphysical metamaterials.

Early researches for tailoring TE fields focus on the decoupled cases, which mean that heat and current flows transport independently without interaction [22–26]. This simplified hypothesis facilitates the generalization of

transformation theory or scattering-cancellation method from extensively studied single physics to multiphysics. Nevertheless, it usually deviates from actual situations because the coupling terms are omitted. Recently, transformed TE metamaterials were reported [27,28], which extended the transformation theory from controlling single field to coupled TE field. The form invariance of TE governing equations under coordinate transformation is verified to remain valid, and the corresponding transformation rules on physical parameters are deduced. However, inhomogeneous and anisotropic TE materials are still required, just as their counterparts in single physics. Although some laminar-structure schemes with natural TE materials are proposed for mimicking the predicated TE parameters [27–30], experimental realization remains lacking due to the complexity in manufacture and availability in materials. Considering the above-mentioned challenges, the scattering-cancellation method, which facilitates manufacture with resulting simplified structures and homogeneous isotropic materials, may be a feasible route for practical implementation in TE control.

In this paper, a bilayer scheme based on the scattering-cancellation method is proposed for manipulating TE

---

[a] E-mail: 18110190048@fudan.edu.cn (corresponding author)
[b] E-mail: jphuang@fudan.edu.cn

fields with naturally occurring TE materials. By introducing an auxiliary generalized potential, we construct Laplacian-form governing equations and derive required thermal conductivities, electrical conductivities, and Seeback coefficients for achieving cloaking, concentrating, and sensing functionalities. Finite-element simulations not only confirm our theoretical design, but also show robustness of the proposed bilayer design under various conditions. Compared with the transformation TE theory, anisotropy and inhomogeneity are no longer necessities, which makes the manufacture more convenient. The theoretical results and device behaviors can be naturally extended to other coupled multiphysics.

Theory. – Let us consider a steady-state TE transport process where physical parameters are scalar at each local position. That is, the isotropy of TE materials is stipulated. In such an isotropic system, the governing equations can be described by [21]

$$\boldsymbol{j} = -\sigma\boldsymbol{\nabla}\mu - \sigma S\boldsymbol{\nabla}T, \tag{1}$$
$$\boldsymbol{\nabla}\cdot\boldsymbol{j} = 0, \tag{2}$$
$$\boldsymbol{q} = -\kappa\boldsymbol{\nabla}T + TS\boldsymbol{j}, \tag{3}$$
$$\boldsymbol{\nabla}\cdot\boldsymbol{q} = -\boldsymbol{\nabla}\mu\cdot\boldsymbol{j}, \tag{4}$$

where $\boldsymbol{q}$ and $\boldsymbol{j}$ are thermal and electric flows, respectively, T and μ refer to temperature and electric potentials, and κ and σ denote scalar thermal and electrical conductivities. S is the Seeback coefficient for coupling heat and current flows. We define U as an auxiliary generalized potential, which is expressed as

$$U = \mu + TS. \tag{5}$$

Combining eqs. (1)–(5), two identical relations about U can be obtained as (a detailed derivation is presented in Part I of the Supplementary Material `Supplementarymaterial.pdf` (SM))

$$\sigma\boldsymbol{\nabla}^2 U = 0 \tag{6}$$

and

$$\kappa\boldsymbol{\nabla}^2 T = \sigma\boldsymbol{\nabla}U\cdot\boldsymbol{\nabla}U. \tag{7}$$

Note that eq. (6) has a Laplacian form, so it is possible to map the field distribution of U by tailoring σ in a bilayer structure with a similar method employed in single-physics cases [12,13]. Then we resort to remolding eq. (7) for detecting the direction relation between $\boldsymbol{\nabla}T$ and $\boldsymbol{\nabla}U$. The Poisson equation (7) has the solution consisting of two parts. One is the general solution of its corresponding Laplace equation

$$\kappa\boldsymbol{\nabla}^2 T = 0. \tag{8}$$

The other is the particular solution. We can see the identical relation

$$\kappa\boldsymbol{\nabla}T = \sigma U\boldsymbol{\nabla}U \tag{9}$$

should always be valid to make eq. (7) be satisfied. This can be deduced by taking the divergence of eq. (9) in both sides as

$$\kappa\boldsymbol{\nabla}^2 T = \sigma\boldsymbol{\nabla}(U\boldsymbol{\nabla}U) = \sigma(\boldsymbol{\nabla}U\cdot\boldsymbol{\nabla}U + U\boldsymbol{\nabla}^2 U) = \sigma\boldsymbol{\nabla}U\cdot\boldsymbol{\nabla}U. \tag{10}$$

Then we can conclude that $\boldsymbol{\nabla}T$ is always parallel to $\boldsymbol{\nabla}U$ in its particular solution. Now we are in the position to discuss the relation between $\boldsymbol{\nabla}T$ and $\boldsymbol{\nabla}U$ in the general solution. T will thus be manipulated like U. Combining eqs. (6) and (8), which are both Laplace equations, we can get the following conditions to make $\boldsymbol{\nabla}T$ parallel to $\boldsymbol{\nabla}U$. Condition I is

$$S = S_0, \tag{11}$$

indicating that S keeps invariant in the whole space. Condition II is

$$\sigma = C\kappa, \tag{12}$$

where C is a constant for keeping σ and κ proportional in the whole space. Condition III relies on boundary condition settings, see Part I of the SM for detailed derivation. It means that external thermal and electrical fields should be parallel for ensuring homodromous $\boldsymbol{\nabla}U$ and $\boldsymbol{\nabla}T$ at each point. These three conditions enable us to map T distribution by tailoring U, which is described by a Laplacian-form governing equation. Then, we can define $f(\boldsymbol{r})$, a coordinate-dependent scalar function, to denote the relationship between $\boldsymbol{\nabla}U$ and $\boldsymbol{\nabla}T$ as

$$\boldsymbol{\nabla}U = f(\boldsymbol{r})\boldsymbol{\nabla}T. \tag{13}$$

Next, we will handle the electrical potential μ. Note that S is constant, by combining eqs. (5) and (13) together, we can obtain

$$\boldsymbol{\nabla}\mu = (f(\boldsymbol{r}) - S)\boldsymbol{\nabla}T. \tag{14}$$

Evidently, $\boldsymbol{\nabla}\mu$ is also parallel to $\boldsymbol{\nabla}T$ and $\boldsymbol{\nabla}U$. So once eqs. (11) and (12) are satisfied simultaneously and the boundary temperature and potential fields are parallel, we are able to manipulate TE flows. Since the bilayer is the most simplified structure for realizing specific functionalities such as cloaking, concentrating, and sensing with isotropic materials in the single field [12,31,32], we design TE cloaking, invisible sensing and concentrating devices with bilayer configurations for verification. More numbers of layers will achieve the same effects, but this cannot improve the behaviors, which has been discussed sufficiently in many single-field metamaterial researches.

To proceed, we design three different functionalities in a size-fixed bilayer structure with background thermal conductivity κ_b and electrical conductivity σ_b, as shown in fig. 1. For simplification without loss of generality, we only consider two-dimensional cases, which can be transferred to three-dimensional systems readily. According to the deductions above, the parameter requirements, *i.e.*, eqs. (11) and (12), should be satisfied simultaneously. And some additional conditions for realizing different functions
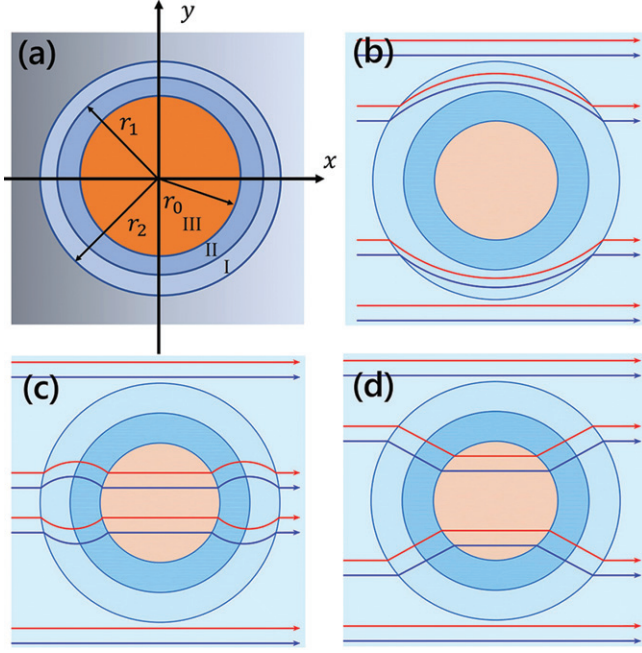
Fig. 1: (a) Schematic diagram of bilayer TE metamaterials. The core is marked as region III with electrical conductivity σ_0 and thermal conductivity κ_0. The inner layer is marked as region II with σ_1 and κ_1. The outer layer is marked as region I with σ_2 and κ_2. The background in gray has σ_b and κ_b. The electrical conductivities, thermal conductivities, and Seeback coefficient S are homogeneous isotropic scalars in each regions. The Cartesian coordinate (x-y) is built on designed metamaterials with overlapped origin and center point. (b) Illustration of a TE cloak. (c) Illustration of a TE invisible sensor. (d) Illustration of a TE concentrator. Red and blue lines represent heat and electrical fluxes respectively in (b)–(d).

are required. We set σ_0, σ_1, σ_2 as respective electrical conductivities from the center to the outer layer. The same definitions are employed for κ_0, κ_1, κ_2. Detailed parameter settings are as follows.

For cloaking [12], which prevents TE flows from running into the center without distorting the ambient temperature and potential distributions outside, as shown in fig. 1(b), the additional conditions for the inner layer should be

$$\sigma_1 \approx 0, \qquad (15)$$

which make the inner layer a nearly perfect thermal/electrical insulation material. And the outer layer should be

$$\sigma_2 = \sigma_b(r_2{}^2 + r_1{}^2)/(r_2{}^2 - r_1{}^2), \qquad (16a)$$

guarantying no distortion of ambient temperature and potential outside.

For invisible sensing [31], which maintains the original temperature and potential in both center and background regions for obtaining accurate sensor effects, as shown in

fig. 1(c), the additional conditions are found as

$$\sigma_1 = \left[\sigma_0 A_3 - \sigma_b A_1 + \sqrt{(\sigma_0 - \sigma_b)(\sigma_0 A_2^2 - \sigma_b A_1^2)}\right] \bigg/ A_5, \qquad (17a)$$

$$\sigma_2 = \left[\sigma_0 A_2 - \sigma_b A_4 - \sqrt{(\sigma_0 - \sigma_b)(\sigma_0 A_2^2 - \sigma_b A_1^2)}\right] \bigg/ A_6, \qquad (17b)$$

where

$$A_1 = r_0^2(r_1^2 + r_2^2) + r_1^2(r_1^2 - 3r_2^2), \qquad (18a)$$

$$A_2 = r_0^2(3r_1^2 - r_2^2) - r_1^2(r_1^2 + r_2^2), \qquad (18b)$$

$$A_3 = r_0^2(2r_0^2 - r_1^2 - r_2^2) + r_1^2(r_1^2 - r_2^2), \qquad (18c)$$

$$A_4 = r_1^2(r_0^2 - r_1^2) + r_2^2(r_0^2 + r_1^2 - 2r_2^2), \qquad (18d)$$

$$A_5 = 2(r_0^2 - r_1^2)(r_0^2 - r_2^2), \qquad (18e)$$

$$A_6 = 2(r_0^2 - r_2^2)(r_1^2 - r_2^2). \qquad (18f)$$

κ_1 and κ_2 follow the formally similar parameter requirements as σ_1 and σ_2. It is noted that two sets of parameters are available in sensing design within a fixed geometry structure. We arbitrarily adopt one of them here.

For concentrating [32], which can enhance the gradients of temperature and potential in the center without distorting the ambient ones, as shown in fig. 1(d), the additional condition for σ_0, σ_1, and σ_2 can be written as

$$\sigma_0 = [r_2^2 r_0^2(\sigma_2 - \sigma_1)(\sigma_2 - \sigma_b)/r_1^2 - r_0^2(\sigma_1 + \sigma_2)(\sigma_b + \sigma_2)$$
$$+ r_1^2(\sigma_1 - \sigma_2)(\sigma_b + \sigma_2) + r_2^2(\sigma_1 + \sigma_2)(\sigma_2 - \sigma_b)]\sigma_1/$$
$$[r_2^2 r_0^2(\sigma_2 - \sigma_1)(\sigma_2 - \sigma_b)/r_1^2 - r_0^2(\sigma_1 + \sigma_2)(\sigma_b + \sigma_2)$$
$$+ r_1^2(\sigma_2 - \sigma_1)(\sigma_b + \sigma_2) - r_2^2(\sigma_1 + \sigma_2)(\sigma_2 - \sigma_b)], \qquad (19)$$

which is obtained by solving the Laplacian equation and then set the coefficient of the nonlinear term of the ambient potential zero. Similar forms of the relation between κ_0, κ_1, and κ_2 are also requested. Given that all the required conditions are met, the ratio of the temperature/potential gradient in the center to the temperature/potential gradient in the background, which can describe the efficiency of concentrating, can be tailored by changing the dimensions and conductivities of the layers. So far, we have listed three sets of parameters for achieving three functionalities in TE transport. It is noted that the rationality of generalization from single physics to coupled multiphysics is established on the basis that eqs. (11) and (12) should be satisfied simultaneously.

Finite-element simulation. – To confirm the proposed theoretical models, we perform finite-element simulations with the commercial software COMSOL Multiphysics [33]. A two-dimensional bilayer structure of $r_0 = 0.02$ m, $r_1 = 0.025$ m, and $r_2 = 0.03$ m is employed. The bilayer structure is embedded at the center of a matrix, whose length is 0.11 m, as shown in fig. 1(a). To demonstrate the functionalities of cloak, invisible sensor and concentrator, respectively, we obtain

Table 1: Simulation parameter settings of TE cloaking, invisible sensing and concentrating functionalities. For simplicity, the Seebeck coefficient is set as 1 in all regions. (This value is much larger than in common materials, which will induce strong coupling effects between heat and electricity.)

	Cloak	Invisible sensor	Concentrator
Thermal conductivity (W/ (m·K))			
κ_0	50	50	0.21
κ_1	0.01	378.5	10
κ_2	554.54	58.5	277
κ_b	100	100	50
Electrical conductivity (S/m)			
σ_0	50	50	0.21
σ_1	0.01	378.5	10
σ_2	554.54	58.5	277
σ_b	100	100	50
Seebeck coefficient (V/m)			
S	1	1	1

three sets of thermal conductivity, electrical conductivity and Seebeck coefficient for each case, listed in table 1. For boundary conditions, temperature and potential gradients should be parallel. So we set boundary conditions as follows. The temperatures of the left and right boundaries are 273.15 K and 333.15 K, respectively, and the potentials of the left and right boundaries are 0 V and 50 V separately. Upper and lower boundaries are thermally and electrically insulated. To show the effectiveness and accuracy of these three metamaterials, we also compare them with bare-perturbation and pure-background results. We perform simulations of these references under the same boundary conditions and plot the temperature and potential distribution of metamaterials and references. Differences of temperature and potential distribution illustrate the changes of temperature and potential between the metamaterials and pure backgrounds. These simulation results of cloak, concentrator and invisible sensor are demonstrated in figs. 2–4.

As shown in figs. 2(d) and (h), 3(d) and (h), 4(d) and (h), both the temperature and potential differences in backgrounds are nearly zero, which means none of these three metamaterials have distorted the ambient temperatures or potentials. This is also confirmed by the overlapping parts of the curves in figs. 2(i) and (j), 3(i) and (j), 4(i) and (j). In contrast, in figs. 2(c) and (g), 3(c) and (g), 4(c) and (g), the ambient temperatures and potentials are manifestly distorted by the bare perturbations. As for the cloak, we can see in figs. 2(a) and (e) or figs. 2(i) and (j), that temperature and potential gradients at the center are nearly zero, which means that thermal and electrical flows are prevented from running into the center. As for the sensor, which refers to the core region coated by the bilayer structure in figs. 3(a) and (e), it can be intuitively seen that the core temperature and potential are consistent before and after the sensor is embedded. In figs. 3(i)
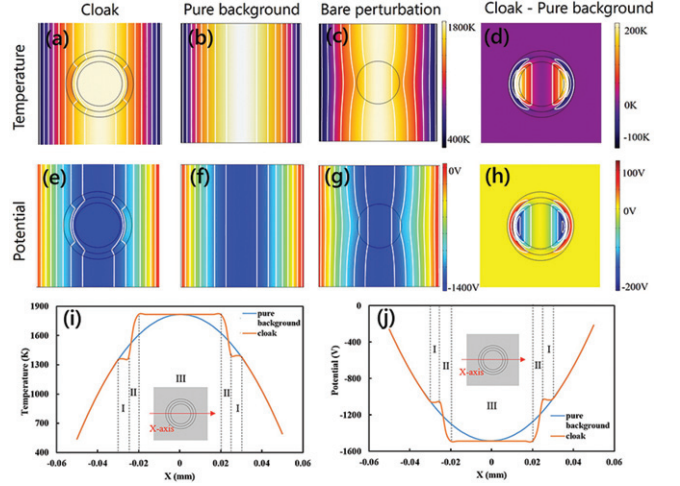

Fig. 2: Simulation results of the TE cloak under parallel external thermal and electrical fields. Isothermal or isopotential lines are marked in white. (a) Temperature distribution of the matrix plus cloak. (b) Temperature distribution of the pure matrix. (c) Temperature distribution of the bare perturbation. (d) Temperature difference distribution between (a) and (b). (e) Potential distribution of the matrix with cloak. (f) Potential distribution of the pure matrix as a reference. (g) Potential distribution of the bare perturbation. (h) Potential difference distribution between (d) and (e). (i) Quantitative temperature comparison between (a) and (b) at the chosen line which crosses the origin along the x-axis. (j) Quantitative potential comparison between (d) and (e) at the chosen line which crosses the origin along the x-axis. Different regions (I, II, and III) are indicated in (i) and (j), corresponding to the model in fig. 1(a). Backgrounds are outside region I.
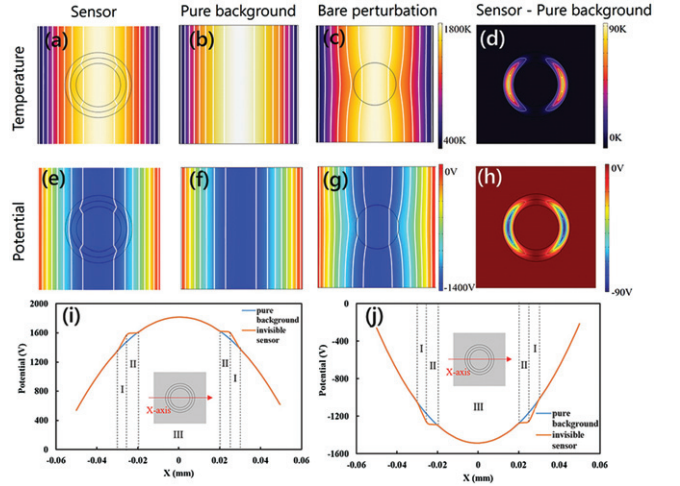

Fig. 3: Simulation results of the TE invisible sensor under parallel thermal and electrical boundary conditions. All figure arrangements are the same as in fig. 2 except the functionality of the central device.

and (j), the curves of metamaterials and references fit well at the core and ambient regions. Therefore, we may safely say that the sensor is able to measure the ambient temperature and potential without introducing any distortion.
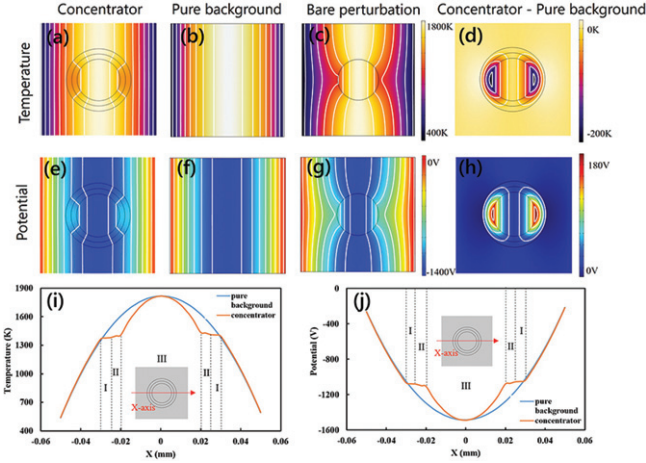
Fig. 4: Simulation results of the TE concentrator under parallel thermal and electrical boundary conditions. All figure arrangements are the same as in fig. 2 except the functionality of the central device.

As for the concentrator, figs. 4(a) and (e) show that both the temperature and potential gradients in the core are greater than the ambient, and from figs. 4(i) and (j), we can see more clearly that along the x-axis, the temperature and potential gradients are enhanced at the center.

To verify that only under the condition ∇T is parallel to $\nabla \mu$ can our design be exactly effective, we perform two simulations for the cloak when ∇T is not parallel to $\nabla \mu$, see fig. 5. In the two upper panels, we set the upper and lower boundary temperatures as 273.15 K and 333.15 K and potentials as 0 V and 50 V, respectively. In the two lower panels, a linear point heat source with power of 6×10^6 Wm^{-3}K^{-1} is applied at the left-bottom corner of the matrix, whose position is $(-0.049$ cm, -0.049 cm). The neighbor sides of the source are insulated, and the temperature of the remaining two sides is kept at 300 K. The results are shown in fig. 5. Along the x-axis, the difference between the ambient temperature (potential) of the pure matrix and matrix with cloak has some minor gaps. This is because the designed schemes are not strictly accurate under nonparallel external fields. But it can still be regarded as a well-approximated result based on the curves in figs. 5(c), (f), (i), and (l), showing great accordance at background regions. The robustness of our design makes it adaptive under multiple complicated conditions.

Discussion and conclusion. – Although actual materials may not perfectly meet the requirements put forward in our theory, we further verify that it is possible that practical realization to an approximate extent can be achieved. See Part II of the SM, where simulations of a TE cylindrical capacitor based on properties of actual ionic conducting TE materials (in solid or quasi-solid state) are executed, approximately achieving the cloaking function. It implies that a small deviation between the ideal properties and actual properties is acceptable. For example, a deviation of 25% between the ideal Seebeck
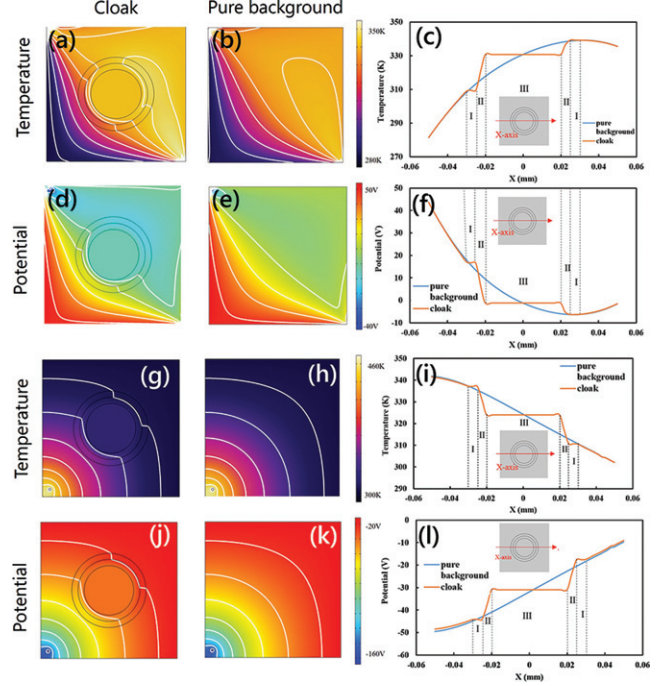

Fig. 5: (a)–(f) Simulation results of the TE cloak under the perpendicular boundary temperature and potential fields. Isothermal or isopotential lines are marked in white. (a) Temperature distribution of the matrix plus cloak. (b) Temperature distribution of the pure matrix. (c) Quantitative temperature comparison between (a) (cloak) and (b) (reference) at the chosen line which crosses the origin along the x-axis. (d) Potential distribution of the matrix with cloak. (e) Potential distribution of the pure matrix. (f) Quantitative potential comparison between (d) (cloak) and (e) (reference) at the chosen line which crosses the origin along the x-axis. Different regions (I, II, and III) are indicated in (g) and (h), corresponding to the model in fig. 1(a). (g)–(l) Simulation results of the TE cloak under the y-direction external potential fields and point heat sources at the left-bottom corner.

coefficient and the actual one has minor impact on the functionality. In fact, many sorts of TE materials such as ionic-conducting materials can yield a large variety of TE characteristics due to various mechanisms and tuning methods such as changing the doping ratio [34] or humidity [35]. Therefore, this provides physical possibility for searching available materials. Comparing with transformation optics which requires extremely anisotropic and inhomogeneous properties, though the proposed scattering cancellation methodology cannot achieve some effects such as rotating, our scheme will yield isotropic and homogeneous parameters to achieve the same effects as cloaking, concentrating, and sensing. Once we have suitable TE materials, the bilayer design will make it much easier to manufacture the corresponding metamaterials. Another issue is that the role of contact resistance, especially the thermal contact resistance (TCR), may affect the practical results [36]. TCR arises as a result of two factors: limited actual contacting areas at interface and lattice mismatch at boundaries of different materials. The latter is

usually too slight to be considered at macroscale according to the acoustic mismatch model or diffusive mismatch model, and the former is usually eliminated by "solid plus soft matter" structures in most reported macroscale experiments. In fact, even without such structures, the experimental results of a decoupled TE sensor, which is based on common metals, are in accord with the theory, ignoring the contact resistance [25].

In conclusion, we have built a scattering-cancellation method for manipulating coupled TE transport and designed three representative devices with bilayer schemes. Considering that TE governing equations are no longer Laplacian forms, additional constraint conditions are required beyond single-field cases. It is noted that our deduced requirements of constant Seebeck coefficient and proportional thermal/electrical conductivities echo with the results of the transformation TE method [27,28] under homogeneous isotropic background conditions. And we further point out that the external TE distribution will not be affected only by applying parallel external thermal and electrical fields on the devices. However, simulation results also verify the robustness of our design under other boundary conditions, which can broaden the practical application range. Our work may provide hints for manipulating coupled multiphysical fields beyond single-physics Laplacian transport, which doubtlessly simplifies the requirements on materials and structures of existing transformation metamaterials. Moreover, since TE effects are widely utilized in practical applications, ranging from generating electric power from waste heat to solid-state–based cooling down, our work may be helpful in facilitating device preparation and raising energy conversion efficiency.

$$* * *$$

Data availability statement: All data that support the findings of this study are included within the article (and any supplementary files).

REFERENCES

[1] Pendry J. B., Schurig D. and Smith D. R., *Science*, **312** (2006) 1780.
[2] Chen H. Y., Chan C. T. and Sheng P., *Nat. Mater.*, **9** (2010) 387.
[3] Pendry J. B., Aubry A., Smith D. R. and Maier S. A., *Science*, **337** (2012) 549.
[4] Xu L. and Chen H. Y., *Nat. Photon.*, **9** (2015) 15.
[5] Yang Z., Mei J., Yang M., Chan N. H. and Sheng P., *Phys. Rev. Lett.*, **101** (2008) 204301.
[6] Zigoneanu L., Popa B. I. and Cummer S. A., *Nat. Mater.*, **13** (2014) 352.
[7] Cummer S. A., Christensen J. and Alù A., *Nat. Rev. Mater.*, **1** (2016) 16001.
[8] Alù A. and Engheta N., *Phys. Rev. E*, **72** (2005) 016623.
[9] Gomory F., Solovyov M., Souc J., Navau C., Prat-Camps J. and Sanchez A., *Science*, **335** (2012) 1466.
[10] Fan C. Z., Gao Y. and Huang J. P., *Appl. Phys. Lett.*, **92** (2008) 251907.
[11] Chen T. Y., Weng C.-N. and Chen J.-S., *Appl. Phys. Lett.*, **93** (2008) 114103.
[12] Han T. C., Bai X., Gao D. L., Thong J. T. L., Li B. W. and Qiu C.-W., *Phys. Rev. Lett.*, **112** (2014) 054302.
[13] Xu H. Y., Shi X. H., Gao F., Sun H. D. and Zhang B. L., *Phys. Rev. Lett.*, **112** (2014) 054301.
[14] Su C., Xu L. J. and Huang J. P., *EPL*, **130** (2020) 34001.
[15] Maldovan M., *Nature*, **503** (2013) 209.
[16] Li Y., Li W., Han T., Zheng X., Li J. X., Li B. W., Fan S. H. and Qiu C.-W., *Nat. Rev. Mater.*, **6** (2021) 488.
[17] Wang J., Dai G. L. and Huang J. P., *iScience*, **23** (2020) 101637.
[18] Yang S., Wang J., Dai G. L., Yang F. B. and Huang J. P., *Phys. Rep.*, **908** (2021) 1.
[19] Bell L. E., *Science*, **321** (2008) 1158899.
[20] Domenicali C. A., *Rev. Mod. Phys.*, **26** (1954) 1103.
[21] Biswas K., He J. Q., Blum I. D., Wu C.-I., Hogan T. P., Seidman D. N., Dravid V. P. and Kanatzidis M. G., *Nature*, **489** (2012) 11439.
[22] Li J.Y., Gao Y. and Huang J. P., *J. Appl. Phys.*, **108** (2010) 074504.
[23] Moccia M., Castaldi G., Savo S., Sato Y and Galdi V., *Phys. Rev. X*, **4** (2014) 021025.
[24] Ma Y. G., Liu Y. C., Raza M., Wang Y. D. and He S. L., *Phys. Rev. Lett.*, **113** (2014) 205501.
[25] Yang T. Z., Bai X., Gao D. L., Wu L. Z., Li B. W., Thong J. T. and Qiu C.-W., *Adv. Mater.*, **27** (2015) 7752.
[26] Lan C. W., Bi K., Fu X. J., Li B. and Zhou J., *Opt. Express*, **24** (2016) 23080.
[27] Stedman T. and Woods L. M., *Sci. Rep.*, **7** (2017) 6988.
[28] Shi W. C., Stedman T. and Woods L., *J. Phys. Energy*, **1** (2019) 025002.
[29] Wang J., Shang J. and Huang J. P., *Phys. Rev. Appl.*, **11** (2019) 024053.
[30] Shi W. C., Stedman T. and Woods L., *J. Appl. Phys.*, **128** (2020) 025104.
[31] Xu L. J., Huang J. P., Jiang T., Zhang L. and Huang J. P., *EPL*, **132** (2020) 14002.
[32] Xu G. Q., Zhou X. and Zhang J. Y., *Int. J. Heat Mass Transfer*, **142** (2019) 118434.
[33] http://www.comsol.com/.
[34] He X., Cheng H., Yue S. and Ouyang J., *J. Mater. Chem. A*, **8** (2020) 10813.
[35] Kim S. L., Lin H. T. and Yu C., *Adv. Energy Mater.*, **6** (2016) 1600546.
[36] Zheng X. and Li B. W., *Phys. Rev. Appl.*, **13** (2020) 024071.